AIAA 99–3254

On Multi-dimensional Unstructured Mesh Adaption

William A. Wood and William L. Kleb
NASA Langley Research Center, Hampton, VA 23681

14th AIAA Computational Fluid Dynamics Conference
June 28–July 1, 1999
Norfolk, VA

On Multi-dimensional Unstructured Mesh Adaption

William A. Wood* and William L. Kleb*
NASA Langley Research Center, Hampton, VA 23681

Anisotropic unstructured mesh adaption is developed for a truly multi-dimensional upwind fluctuation splitting scheme, as applied to scalar advection-diffusion. The adaption is performed locally using edge swapping, point insertion/deletion, and nodal displacements. Comparisons are made versus the current state of the art for aggressive anisotropic unstructured adaption, which is based on *a posteriori* error estimates. Demonstration of both schemes to model problems, with features representative of compressible gas dynamics, show the present method to be superior to the *a posteriori* adaption for linear advection. The performance of the two methods is more similar when applied to nonlinear advection, with a difference in the treatment of shocks. The *a posteriori* adaption can excessively cluster points to a shock, while the present multi-dimensional scheme tends to merely align with a shock, using fewer nodes. As a consequence of this alignment tendency, an implementation of eigenvalue limiting for the suppression of expansion shocks is developed for the multi-dimensional distribution scheme. The differences in the treatment of shocks by the adaption schemes, along with the inherently low levels of artificial dissipation in the fluctuation splitting solver, suggest the present method is a strong candidate for applications to compressible gas dynamics.

Nomenclature

$\vec{A}$	Flux Jacobian
E_r	Error estimate
$\vec{F}$	Flux function
ℓ	Edge length
$\hat{n}$	Outward unit normal
$\vec{r}$	Position vector
S	Area of a triangle
t	Time
U	Dependent variable
α, β	Curvilinear advection speeds
ε	Eigenvalue limiting parameter
$\vec{\lambda}$	Advection velocity
μ	Diffusion coefficient
ϕ	Fluctuation
ϕ^ξ, ϕ^η	Fluctuation components
$\phi^{*^\xi}, \phi^{*^\eta}$	Limited fluctuations
$\phi'^\epsilon, \phi'^\eta$	Artificial dissipation terms
ϕ^v	Diffusive fluctuation
ψ	Limiter function
Υ	Minimization functional
Ξ	Weighting matrix
Ω	General element area
$\vec{\nabla}$	Gradient operator
Δ^n	Forward difference in iterate n

Subscripting independent variables represents differentiation. Tildes indicate averaged states with Property U. Over-bar indicates cell-averaged value.

*Aerospace Engineer, Aerothermodynamics Branch, Aero- and Gas-Dynamics Division.

Introduction

HIGH-FIDELITY aerothermodynamic analyses for hypersonic vehicles, such as the X-34, can require up to 390 CPU hours on a Cray C-90 for a single computational fluid dynamics (CFD) solution, even when using a modern, proven, highly-tuned solver.[1] The associated solution-adapted grids include up to 9 million nodes. It is desired to reduce solution times by more than an order of magnitude so as to increase the relevancy of CFD to the national X-plane programs. Reducing the required mesh sizes, while maintaining or improving accuracy, has been targeted as a high-payoff endeavor for minimizing the cost of computational aerothermodynamics. Fundamental algorithmic advances for both the flow solver and the mesh-adaption strategy will contribute to reduced costs.

Solution-adaptive remeshing techniques have been utilized with some success for hypersonic flows on structured domains. A leader in this field is Gnoffo,[2] who utilizes a spring analogy energy minimization to align the bow shock and cluster to the boundary layer. This approach works very well for entry forebodies, for which it was developed, but is more difficult to apply to complex vehicle shapes. The method also is unresponsive to embedded shocks or other shock-layer flow features.

Harvey[3,4,5] has developed a mesh adaption technique that is sensitive to shock-layer features to obtain parabolized Navier-Stokes solutions over simple configurations, *e.g.* cones, using a spring analogy based

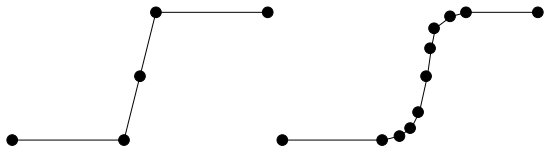

Fig. 1 Pictorial of 'ideal' mesh for shock discontinuity (left) and mesh resulting from curvature-based clustering (right).

on Gnoffo's work. Unfortunately, defining relative clustering strengths for various flow features proved difficult, and a damaging lack of robustness is shown for three-dimensional leeside flowfields.[4]

Mesh adaption on unstructured domains offers a significant benefit over structured mesh adaption—the ability to locally insert and delete nodes. Much of the research in this area has gone into global remeshing using isotropic cells.[6,7,8,9,10,11] Grids composed of (nearly) isotropic cells quickly become prohibitively large for hypersonic applications, where the capture of essentially one-dimensional flow features, such as shocks, requires refinement in all three spatial dimensions.

More recently, impressive results using anisotropic elements have been reported by Habashi *et al.*[12,13,14,15,16,17] With their approach, all grid adaptions are local operations, as opposed to global remeshings. Highly-stretched elements are obtained, achieved by equating the interpolation error along each edge, again using a spring analogy minimization. The clustering is driven by *a posteriori* error estimation based on second derivatives of the solution. This sort of clustering is intended to reduce the interpolation error in a piecewise-linear data representation,[18,19] but is not necessarily driven by the flow physics, and can lead to excessive clustering or conflicting requirements in certain regions, such as a bow shock or stagnation point. Figure 1 presents an illustrative pictorial based on the results of Ait-Ali-Yahia *et al*,[20] where 18 cells were driven into the bow shock by gradient based clustering. A shock is pictured on the left side of the figure with an ideal mesh for a three-point stencil. On the right-hand side is a mesh dictated by curvature-based clustering, clearly containing more points than necessary.

Roe[21,22] has applied the concept of local node movements to a scalar advection problem using a fluctuation splitting solver. His analysis reveals that a characteristic mesh results, with far fewer points required than curvature clustering would imply. His method is based on the minimization of an objective function formed by taking derivatives of the fluctuation splitting scheme. A differentiable high-resolution linear scheme, which in general cannot be monotonic,[23] was chosen. For a complex solution field or for systems of equations it may not be possible to achieve a perfectly-aligned characteristic mesh, in which case the non-monotonic property would most likely be detrimental or even fatal to the solution. It is not clear how to extend the differentiability requirement to a high-resolution, non-linear monotonic scheme.

The current study seeks to borrow from the full suite of aggressive anisotropic unstructured mesh adaptions that have been developed for traditional finite volume or finite element methods, and to apply them in novel ways to the inherently multi-dimensional fluctuation splitting distribution scheme. Prior work[24,25] has shown fluctuation splitting can deliver greater accuracy on coarser meshes than finite volume when applied to model problems with features representative of those present in hypersonic flows. A mesh adaption strategy developed in conjunction with fluctuation splitting that is robust and general yet does not overly cluster to shocks could contribute significantly to lowering the cost of computational aerothermodynamics.

This paper judges the potential of such an adaption strategy for a fluctuation splitting solver by comparing its performance versus a state-of-the-art solution-adaptive strategy, based on *a posteriori* error estimates for a finite volume solver, as applied to several scaler model problems representative of some of the features present in compressible gas dynamics. The governing equations are stated along with a brief outline of the finite volume and fluctuation splitting discretizations. Descriptions of the *a posteriori* error estimation and the basic local adaption techniques are followed by details of the adaption strategy developed for the present study, constructed as a series of minimization operations on the cell fluctuations. Applications to linear advection, non-linear advection, and advection-diffusion lead to conclusions about the suitability of the present method for extension to compressible gas dynamics.

Governing Equations

The scalar advection-diffusion equation,

$$U_t + \vec{\nabla}\cdot\vec{F} = \vec{\nabla}\cdot(\mu\vec{\nabla}U) \tag{1}$$

is considered in two spatial dimensions on triangulated unstructured domains. The physical domain is chosen to be the unit square in the second quadrant. Steady-state solutions are sought through pseudo-time relaxation.

A linear equation is obtained with,

$$\vec{F} = \vec{\lambda}U \tag{2}$$

while non-linear advection is obtained with,

$$\vec{F} = (\frac{1}{2}U^2,\, U)\ , \qquad \mu = 0 \tag{3}$$

Finite Volume

The finite volume discretization is constructed as an edge-based implementation of the approximate Riemann solver due to Roe.[26] The numerical flux at a

median-dual control-volume face is,

$$\frac{1}{2}\left(\vec{F}_{in}+\vec{F}_{out}\right)\cdot\hat{n}-\frac{1}{2}|\tilde{\vec{A}}\cdot\hat{n}|(U_{out}-U_{in}) \qquad (4)$$

with the flux Jacobian defined,

$$\tilde{\vec{A}}=\frac{\partial\vec{F}}{\partial U} \qquad (5)$$

Node-based limited reconstruction for second-order accuracy follows Barth,[27]

$$U_{face}=U_0+\psi(\vec{\nabla}U)_0\cdot\vec{r} \qquad (6)$$

Diffusion terms are discretized as a finite element distribution such that the contribution to node i of a triangle is given by,

$$\phi_i^v=-\frac{\bar{\mu}\ell_i}{4S}\sum_{j=1}^{3}U_j\ell_j\hat{n}_j\cdot\hat{n}_i \qquad (7)$$

with the convention that edge i is opposite to node i.

Fluctuation Splitting

The fluctuation splitting discretization is the multi-dimensional upwind residual distribution scheme of Sidilkover.[28] The advective fluctuation is defined on a triangular cell,

$$\phi=-\int_\Omega\vec{\nabla}\cdot\vec{F}\,d\Omega=\phi^\xi+\phi^\eta \qquad (8)$$

where,

$$\phi^\xi=\alpha(U_1-U_2),\qquad \phi^\eta=\beta(U_3-U_2) \qquad (9)$$

and,

$$\alpha=\frac{\ell_1}{2}\tilde{\vec{A}}\cdot\hat{n}_1,\qquad \beta=\frac{\ell_3}{2}\tilde{\vec{A}}\cdot\hat{n}_3 \qquad (10)$$

The fluctuations are limited to achieve linearity preservation as,

$$\begin{aligned}\phi^{*^\xi}&=\phi^\xi+\psi\left(\frac{-\phi^\xi}{\phi^\eta}\right)\phi^\eta\\ \phi^{*^\eta}&=\phi^\eta-\psi\left(\frac{-\phi^\xi}{\phi^\eta}\right)\phi^\eta\end{aligned} \qquad (11)$$

and artificial dissipation is introduced for upwind monotonicity,

$$\phi'^\xi=\mathrm{sign}(\alpha)\phi^{*^\xi},\qquad \phi'^\eta=\mathrm{sign}(\beta)\phi^{*^\eta} \qquad (12)$$

Expansion shocks are eliminated by extending the one-dimensional eigenvalue limiting of Harten and Hymen[29] to multiple dimensions by searching for expansions in the ξ and η directions separately. The artificial dissipation can be recast, with Eqn. 9, as,

$$\begin{aligned}\phi'^\xi&=|\alpha|(U_1-U_2)+\mathrm{sign}(\alpha)\psi\phi^\eta\\ \phi'^\eta&=|\beta|(U_3-U_2)-\mathrm{sign}(\beta)\psi\phi^\eta\end{aligned} \qquad (13)$$

The absolute values of the advection speeds are limited as,

$$|\alpha|=\begin{cases}|\alpha| & \text{if } |\alpha|\geq\varepsilon_{(\alpha)}\\ \frac{\alpha^2+\varepsilon_{(\alpha)}^2}{2\varepsilon_{(\alpha)}} & \text{if } |\alpha|<\varepsilon_{(\alpha)}\end{cases} \qquad (14)$$

and similarly for $|\beta|$. The small parameters for Eqn. 14 are obtained as,

$$\begin{aligned}\epsilon_{(\alpha)}&=\frac{1}{2}\max\left[0,\ell_1\hat{n}_1\cdot(\tilde{\vec{A}}-\vec{A}_1),\ell_1\hat{n}_1\cdot(\vec{A}_2-\tilde{\vec{A}})\right]\\ \epsilon_{(\beta)}&=\frac{1}{2}\max\left[0,\ell_3\hat{n}_3\cdot(\vec{A}_2-\tilde{\vec{A}}),\ell_3\hat{n}_3\cdot(\tilde{\vec{A}}-\vec{A}_3)\right]\end{aligned} \qquad (15)$$

The advective fluctuations are distributed to the nodes of the triangle as,

$$\begin{aligned}\text{node 1}&\leftarrow\frac{1}{2}(\phi^{*^\xi}-\phi'^\xi)\\ \text{node 2}&\leftarrow\frac{1}{2}(\phi^{*^\xi}+\phi'^\xi)+\frac{1}{2}(\phi^{*^\eta}+\phi'^\eta)\\ \text{node 3}&\leftarrow\frac{1}{2}(\phi^{*^\eta}-\phi'^\eta)\end{aligned} \qquad (16)$$

Diffusive terms are computed as a finite element discretization and distributed as in Eqn. 7.

Further details of the specific implementations for both the finite volume and fluctuation splitting schemes can be found in Ref. 25.

It will be demonstrated that fluctuation splitting can provide exact solutions to multi-dimensional linear advection problems, Eqns. 1 and 2 with $\mu=0$, on a properly aligned mesh. The counter-case, of a poorly aligned mesh producing significant artificial cross-diffusion, has been covered in Ref. 24.

The construction of a properly aligned mesh begins by looking at the elemental fluctuation, Eqn. 8, which can be written,

$$\phi=\frac{1}{2}\left[(U_1-U_2)\ell_1\hat{n}_1+(U_3-U_2)\ell_3\hat{n}_3\right]\cdot\tilde{\vec{\lambda}} \qquad (17)$$

If one edge of the triangular element, without loss of generality say edge 1 (edge 1 is opposite to node 1), is parallel to the cellular advection velocity, then $\hat{n}_1\cdot\tilde{\vec{\lambda}}=0$, and the fluctuation reduces to,

$$\phi=\frac{1}{2}\tilde{\vec{\lambda}}\cdot\hat{n}_3\ell_3(U_3-U_2) \qquad (18)$$

Now $\phi\rightarrow 0$ as $U_2\rightarrow U_3$, irrespective of the value of U_1. Since the artificial dissipation scales proportionally with the cell fluctuation, the exact isentropic solution will be captured as the fluctuation splitting scheme converges to $U_2=U_3$.

A mesh such that each cell has one edge aligned with its averaged advection velocity is analogous to a characteristic mesh. Unfortunately, this edge-alignment concept will not, in general, produce an exact solution in the presence of physical diffusion because the correct

result will typically be $U_2 \neq U_3$ even if edge 1 is aligned with $\tilde{\vec{\lambda}}$. Additionally, extensions to systems possessing multiple or imaginary characteristics are difficult to conceive.

Curvature Clustering

Current state of the art for local unstructured mesh adaption is based on *a posteriori* error estimation.[6,7,10,11,19,12,15,16,17,30] The error estimates can be derived either by looking at the leading truncation error terms in the spatial discretization or by considering the solution interpolation error. In practice, either approach reduces, for second-order-accurate spatial discretizations, to a check on the curvature of the solution. If isotropic cells are desired, the magnitude of the local curvature inversely dictates the element sizes, while for anisotropic adaption directional derivatives can be used to stretch elements.

Habashi[17] defines the *a posteriori* error estimate on an edge to vary like,

$$|E_r| \sim \ell^2 \left| \frac{\partial^2 U}{\partial r^2} \right| \tag{19}$$

or as "the edge length squared times the second derivative of the solution." In the finite volume context, one simple and efficient way to construct an edge-based error estimate along edge $\overline{01}$ is,

$$\begin{aligned} |E_r| &\sim \left| \frac{\vec{\nabla} U_1 \cdot \frac{\vec{r}_{01}}{\ell_{01}} - \vec{\nabla} U_0 \cdot \frac{\vec{r}_{01}}{\ell_{01}}}{\ell_{01}} \right| \ell_{01}^2 \\ &= \left| \left(\vec{\nabla} U_1 - \vec{\nabla} U_0 \right) \cdot \vec{r}_{01} \right| \end{aligned} \tag{20}$$

Barth's edge-based finite volume scheme, used here, already requires the gradient computations, making the error estimate a trivial step.

Having defined an error estimate for all edges, the adaption strategy seeks to reduce the magnitude of the estimates while anisotropically stretching cells to equidistribute the error across all edges. The adaption is performed locally using the four basic operations: edge swapping, point deletion, point insertion, and nodal displacement.

One simple method to improve a mesh is to swap edges between nodes, altering the local connectivity. If the triangles to either side of an edge form a convex quadrilateral, then that edge is a candidate to be swapped. If the error estimate for the swapped connectivity is smaller than for the current edge connectivity, then the edge is swapped. In practice, an error threshold is employed with all the local operations discussed herein to avoid limit cycles in smooth regions of the solution.

If all edges emanating from a node have very small error estimates, then that node is deleted. If a given edge has an excessively large error, then that edge is split by adding a node at the midpoint.

The approach for moving nodes uses the spring analogy, similar to the techniques presented by Gnoffo[2] and Ait-Ali-Yahia *et al.*[20] The springs are taken to be the mesh edges. The spring constants are the edge error estimates. A minimization is then sought for a potential energy formed as,

$$\sum_j \frac{1}{2} |E_r|_j \, \vec{r}_{0j}^{\,2} \tag{21}$$

where j represents all distance-one neighbors to node 0. The minimum is obtained by setting the derivative to zero, giving the requirement,

$$\sum_j |E_r|_j \, \vec{r}_{0'j} = 0 \tag{22}$$

where $0'$ indicates the new, minimum energy position of node 0. Holding the edge error estimate constant during the displacement, an updated position vector can be obtained,

$$\sum_j |E_r|_j \, (\vec{r}_{0j} + \vec{r}_{0'0}) = 0 \tag{23}$$

$$\vec{r}_{00'} = -\vec{r}_{0'0} = \frac{\sum_j |E_r|_j \, \vec{r}_{0j}}{\sum_j |E_r|_j} \tag{24}$$

Equation 24 gives the position vector pointing from the current location of node 0 to its adapted location. This adapted location is an attempt to optimally equate the scaled error estimates over all edges connected to the current node.

Following the recommendations of Dompierre *et al*[12] and Habashi *et al*,[17] the nodal displacement technique is used as a smoother between applications of point insertion/deletion and edge swapping. Coupling between the solver and the mesh adaptor is maintained by iterating the solver between adaption operations. A complete adaption cycle consists of the following steps:

Solve on initial mesh.

Swap diagonals and iterate solver.

Move nodes and iterate solver.

Insert nodes and iterate solver.

Move nodes and iterate solver.

Delete nodes and iterate solver.

Swap diagonals and iterate solver.

Move nodes and iterate solver.

The preceding steps are repeated until convergence of the entire process.

Fluctuation Minimization

Fluctuation splitting, being a distribution scheme, discretizes the partial differential equation into a set of algebraic relations for the nodal values of the dependent variable. Convergence of the solver implies that the nodal updates for U are driven to zero. However,

the nodal updates are formed as contributions from all surrounding cells, and the fluctuations defined on these cells are not necessarily reduced toward zero, as the possibility exists for positive and negative contributions from neighboring cells to cancel on summation about a node.

Recall that the fluctuation splitting artificial dissipation terms, Eqn. 12, scale with the cell's fluctuation, and that for linear advection it is possible to eliminate the production of artificial dissipation by using an appropriately designed mesh. Explicitly adapting a mesh to align with characteristic directions proves awkward to translate into an algorithm, and offers limited hope for extending to diffusive problems or systems.

An alternative tact is chosen whereby the mesh is adapted so that the solver will minimize both the cell fluctuations, and hence the artificial dissipation, as well as the nodal updates. Since there are on the order of twice as many cells as nodes, the fluctuations are minimized in a least-squares sense. The advantage of fluctuation-based, rather than characteristic-based, adaption is that the fluctuations remain defined for diffusive problems and systems.

Given a sub-optimal mesh and solution corrupted with artificial dissipation, the present adaption method performs a series of local operations, driven by predictions of what the fluctuations will be on the modified mesh. The sequence of local optimizations is iterated to obtain globally improved solutions.

For edge swapping, the root mean square (RMS) of the fluctuations to either side of the edge is compared to the RMS of the fluctuations in the swapped configuration. If the swapped RMS is lower, then the edge is swapped. If the fluctuations in all cells surrounding a node are very small and the fluctuations will remain small in the re-triangulated region without that node, then the node is deleted. If the fluctuations in the two cells to either side of an edge are very large, then that edge is split by adding a node at the midpoint.

For displacing nodes, a scheme to minimize RMS of fluctuations has been presented by Roe.[21,22] The development presented by Roe uses the same minimization scheme to evolve the solution as is used to drive the nodal positioning. That type of fluctuation splitting solver has a central difference flavor and is not monotonic. The present procedure incorporates the upwind, non-linear fluctuation splitting algorithm of Sidilkover into some of the mesh movement strategies of Roe.

At a given node, the nodal displacement is computed as a first step and then the solution is updated at the new nodal location *via* a local point-implicit inversion. In this manner a global mesh movement sweep can be accomplished in conjunction with a single Gauß-Seidel iteration of the solver. In this section the current node to be moved is globally numbered node i. Within each triangular element the nodes are locally numbered 1–3. Derivatives in y are omitted when they exactly follow from the derivatives in x.

The functional to be minimized is defined at the node as a sum of contributions from all cells surrounding the node (equivalent to Eqn. 13, p. 248 in Ref. 22),

$$\Upsilon_i = \frac{1}{2} \sum_{\mathsf{T}} \Xi_{\mathsf{T}} \phi_{\mathsf{T}}^2 \tag{25}$$

for all triangles T containing node i. The weighting factor, Ξ_{T}, is a positive scalar, generalizing to a symmetric, positive definite matrix for systems. The functional is thus a sum of positive semi-definite contributions from triangles containing the current node.

The derivative of Υ with respect to a nodal coordinate is,

$$\frac{\partial \Upsilon_i}{\partial x_i} = \sum_{\mathsf{T}} \left(\frac{\phi_{\mathsf{T}}^2}{2} \frac{\partial \Xi_{\mathsf{T}}}{\partial x_i} + \Xi_{\mathsf{T}} \phi_{\mathsf{T}} \frac{\partial \phi_{\mathsf{T}}}{\partial x_i} \right) \tag{26}$$

Note that the derivatives in Eqn. 26 represent the change in solution values as the discrete mesh is perturbed, and as such are to be interpreted in the context of variational calculus, and not as spatial gradients according to the more-familiar multi-variable calculus.

The minimization of Υ can be performed using a fixed-point iteration to force the derivatives to zero,

$$x_i^{n+1} = x_i^n - \frac{\partial \Upsilon}{\partial x_i}, \qquad \Delta^n x_i = -\frac{\partial \Upsilon}{\partial x_i} \tag{27}$$

Equation 27 can be combined with Eqn. 26 in the form of a distribution method of steepest descent,

$$\Delta^n x_i \leftarrow -\frac{\phi_{\mathsf{T}}^2}{2} \frac{\partial \Xi_{\mathsf{T}}}{\partial x_i} - \Xi_{\mathsf{T}} \phi_{\mathsf{T}} \frac{\partial \phi_{\mathsf{T}}}{\partial x_i} \tag{28}$$

Convergence can be enhanced over the fixed-point iteration by using a Newton scheme. Expanding the gradient in an approximate Taylor series,

$$\begin{aligned} 0 = \left. \frac{\partial \Upsilon}{\partial x_i} \right|^{n+1} &\simeq \left. \frac{\partial \Upsilon}{\partial x_i} \right|^{n} + \Delta^n x_i \frac{\partial}{\partial x_i} \left(\left. \frac{\partial \Upsilon}{\partial x_i} \right|^{n} \right. \\ &\quad + \Delta^n y_i \frac{\partial}{\partial y_i} \left(\left. \frac{\partial \Upsilon}{\partial x_i} \right|^{n} \right. \end{aligned} \tag{29}$$

$$\begin{aligned} 0 = \left. \frac{\partial \Upsilon}{\partial y_i} \right|^{n+1} &\simeq \left. \frac{\partial \Upsilon}{\partial y_i} \right|^{n} + \Delta^n x_i \frac{\partial}{\partial x_i} \left(\left. \frac{\partial \Upsilon}{\partial y_i} \right|^{n} \right. \\ &\quad + \Delta^n y_i \frac{\partial}{\partial y_i} \left(\left. \frac{\partial \Upsilon}{\partial y_i} \right|^{n} \right. \end{aligned} \tag{30}$$

leading to the form,

$$\Delta^n \begin{Bmatrix} x_i \\ y_i \end{Bmatrix} = - \begin{bmatrix} \frac{\partial^2 \Upsilon}{\partial x_i^2} & \frac{\partial^2 \Upsilon}{\partial x_i \partial y_i} \\ \frac{\partial^2 \Upsilon}{\partial x_i \partial y_i} & \frac{\partial^2 \Upsilon}{\partial y_i^2} \end{bmatrix}^{-1} \begin{Bmatrix} \frac{\partial \Upsilon}{\partial x_i} \\ \frac{\partial \Upsilon}{\partial y_i} \end{Bmatrix} \tag{31}$$

In Ref. 21, Roe suggests neglecting the off-diagonal terms in Eqn. 31.

Second derivatives of the objective function are,

$$\frac{\partial^2 \Upsilon}{\partial x_i^2} = \sum_{\mathsf{T}} \left[\frac{\phi_{\mathsf{T}}^2}{2} \frac{\partial^2 \Xi_{\mathsf{T}}}{\partial x_i^2} + 2\phi_{\mathsf{T}} \Xi_{\mathsf{T}} \frac{\partial \Xi_{\mathsf{T}}}{\partial x_i} \frac{\partial \phi_{\mathsf{T}}}{\partial x_i} + \Xi_{\mathsf{T}} \left(\frac{\partial \phi_{\mathsf{T}}}{\partial x_i} \right)^2 + \Xi_{\mathsf{T}} \phi_{\mathsf{T}} \frac{\partial^2 \phi_{\mathsf{T}}}{\partial x_i^2} \right] \tag{32}$$

$$\frac{\partial^2 \Upsilon}{\partial x_i \partial y_i} = \sum_{\mathsf{T}} \left[\phi_{\mathsf{T}} \left(\frac{\partial \phi_{\mathsf{T}}}{\partial x_i} \frac{\partial \Xi_{\mathsf{T}}}{\partial y_i} + \frac{\partial \Xi_{\mathsf{T}}}{\partial x_i} \frac{\partial \phi_{\mathsf{T}}}{\partial y_i} \right) + \frac{\phi_{\mathsf{T}}^2}{2} \frac{\partial^2 \Xi_{\mathsf{T}}}{\partial x_i \partial y_i} + \Xi_{\mathsf{T}} \frac{\partial \phi_{\mathsf{T}}}{\partial x_i} \frac{\partial \phi_{\mathsf{T}}}{\partial y_i} + \phi_{\mathsf{T}} \Xi_{\mathsf{T}} \frac{\partial^2 \phi_{\mathsf{T}}}{\partial x_i \partial y_i} \right] \tag{33}$$

Explicit expressions for the derivatives of the fluctuations are grouped in the appendix. For application to fluctuation splitting schemes other than Sidilkover's, only those equations in the appendix would change.

For Ξ, Roe[22] chooses $\Xi_{\mathsf{T}} = \frac{1}{S_{\mathsf{T}}}$, for which the derivatives are,

$$\frac{\partial \Xi_{\mathsf{T}}}{\partial x_i} = -\frac{1}{S_{\mathsf{T}}^2} \frac{\partial S_{\mathsf{T}}}{\partial x_i} \tag{34}$$

$$\frac{\partial^2 \Xi_{\mathsf{T}}}{\partial x_i^2} = \frac{2}{S_{\mathsf{T}}^3} \left(\frac{\partial S_{\mathsf{T}}}{\partial x_i} \right)^2 - \frac{1}{S_{\mathsf{T}}^2} \frac{\partial^2 S_{\mathsf{T}}}{\partial x_i^2} \tag{35}$$

$$\frac{\partial^2 \Xi_{\mathsf{T}}}{\partial x_i \partial y_i} = \frac{2}{S_{\mathsf{T}}^3} \frac{\partial S_{\mathsf{T}}}{\partial x_i} \frac{\partial S_{\mathsf{T}}}{\partial y_i} - \frac{1}{S_{\mathsf{T}}^2} \frac{\partial^2 S_{\mathsf{T}}}{\partial x_i \partial y_i} \tag{36}$$

The area of a triangle is,

$$S_{\mathsf{T}} = \frac{1}{2} \left[x_1(y_2 - y_3) + x_2(y_3 - y_1) + x_3(y_1 - y_2) \right] \tag{37}$$

leading to the derivatives,

$$\frac{\partial S_{\mathsf{T}}}{\partial x_2} = \frac{y_3 - y_1}{2} \qquad \frac{\partial S_{\mathsf{T}}}{\partial y_2} = \frac{x_1 - x_3}{2} \tag{38}$$

and,

$$\frac{\partial^2 S_{\mathsf{T}}}{\partial x_2^2} = \frac{\partial^2 S_{\mathsf{T}}}{\partial y_2^2} = \frac{\partial^2 S_{\mathsf{T}}}{\partial x_2 \partial y_2} = 0 \tag{39}$$

This choice of weighting emphasizes fluctuations on the smaller cells.

An alternative is to weight all cells equally, with Ξ_{T}=1. Two other obvious choices for weighting are Ξ_{T}=S_{T}, emphasizing fluctuations on the larger cells, and $\Xi_{\mathsf{T}} = \frac{1}{S_{\mathsf{T}}^2}$, for even stronger emphasis on the smaller cells. The derivatives for this latter case are, with Eqn. 39,

$$\frac{\partial \Xi_{\mathsf{T}}}{\partial x_i} = -\frac{2}{S_{\mathsf{T}}^3} \frac{\partial S_{\mathsf{T}}}{\partial x_i} \tag{40}$$

$$\frac{\partial^2 \Xi_{\mathsf{T}}}{\partial x_i^2} = \frac{6}{S_{\mathsf{T}}^4} \left(\frac{\partial S_{\mathsf{T}}}{\partial x_i} \right)^2 \tag{41}$$

$$\frac{\partial^2 \Xi_{\mathsf{T}}}{\partial x_i \partial y_i} = \frac{6}{S_{\mathsf{T}}^4} \frac{\partial S_{\mathsf{T}}}{\partial x_i} \frac{\partial S_{\mathsf{T}}}{\partial y_i} \tag{42}$$

A complete adaption cycle follows the same steps as outlined for curvature-clustering adaption.

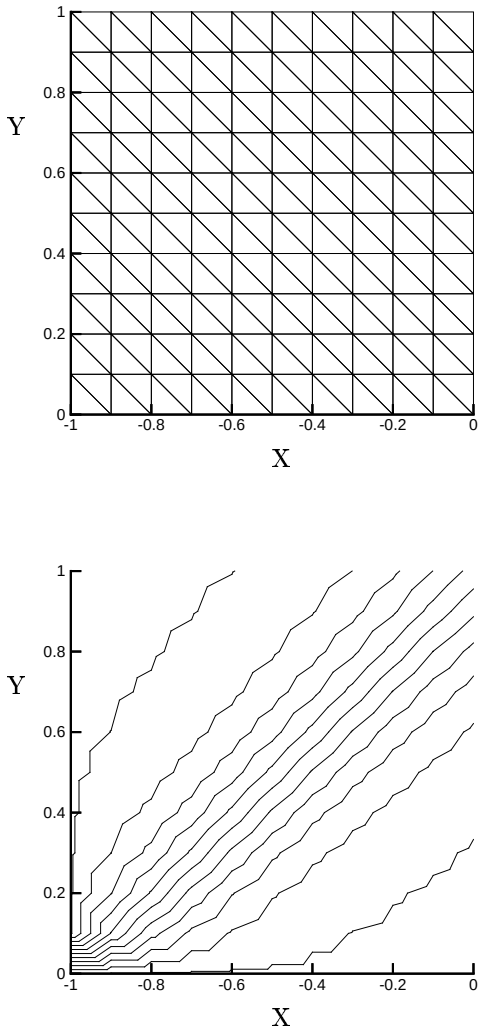

Fig. 2 Unadapted finite volume results for linear advection of shear. Solution contours vary on (0,1) with 0.1 increments.

Results

Four scalar test cases are considered: uniform advection, circular advection, non-linear advection, and advection-diffusion. The emphasis of the current study is to evaluate the performance of the adaption schemes using only a few adaption cycles, typically 1–4, on each case. In this manner, significant improvements in the solutions are sought with little additional overhead from the adaptions. It should be noted that continued application of either adaption strategy would lead to continually refined solutions, though at the cost of ever increasing numbers of nodes.

Linear Advection

The first test case is for linear advection of a shear discontinuity at 45°, $\vec{\lambda}$=(1,1). Inflow conditions are $U(-1, y) = 0$, $U(x, 0) = 1$. The starting 121-node

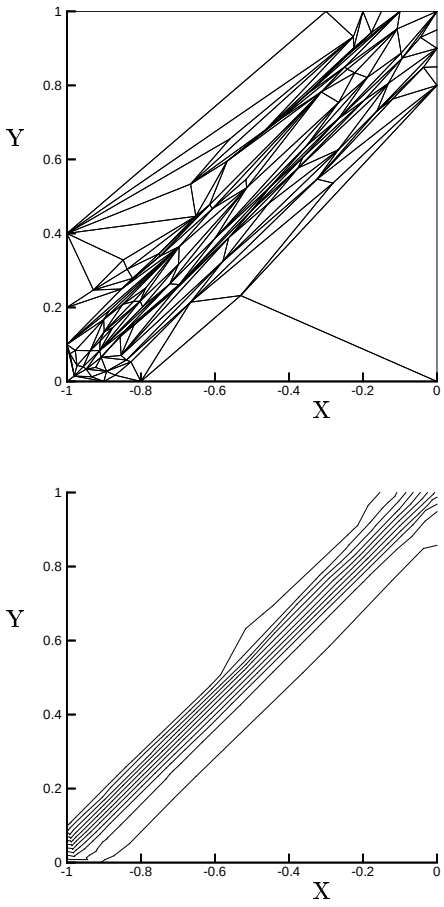

Fig. 3 Adapted mesh with greatly improved finite volume solution for 45° shear. Solution contours vary on (0,1) with 0.1 increments.

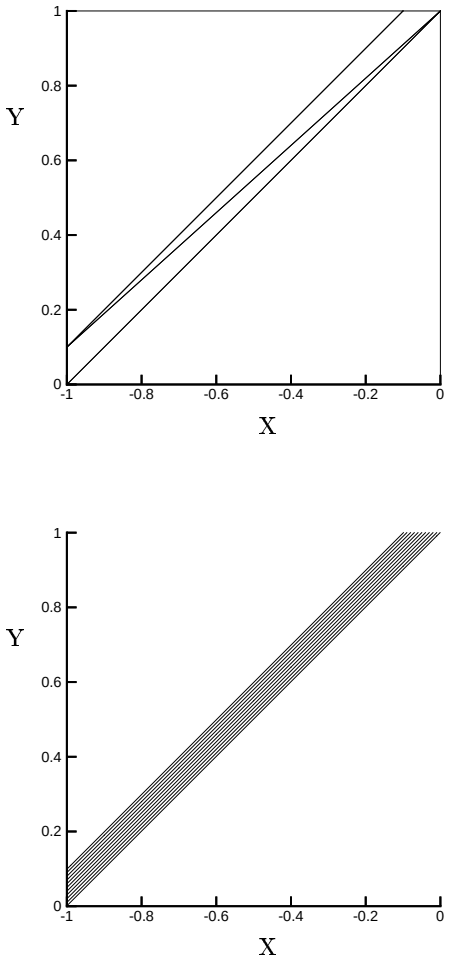

Fig. 4 Optimal fluctuation splitting adaption and exact solution for 45° shear case.

mesh and converged finite volume solution, using the compressive van Albada limiter, are shown in Fig. 2. Excessive spreading of the contour lines, indicative of the magnitude of non-physical dissipation corrupting the solution, is seen. The fluctuation splitting solution on this mesh, using the Minmod limiter, is similar in character, though somewhat less diffusive,[31] to the finite volume solution.

Four cycles of the curvature-clustering adaption with the finite volume solver result in the 103-node mesh and solution of Fig. 3. While the adapted mesh is highly anisotropic, a significant improvement in resolution of the shear has been obtained with a 15 percent reduction in the number of nodes.

However, a single application of only the edge-swapping and point-deletion routines with the fluctuation splitting solver results in the optimal mesh and exact solution, Fig. 4, obtained with no interior nodes. The six retained boundary nodes are a 95 percent reduction in the number of nodes. Applying the finite volume solver to this optimal fluctuation splitting mesh gives the diffused result of Fig. 5, showing

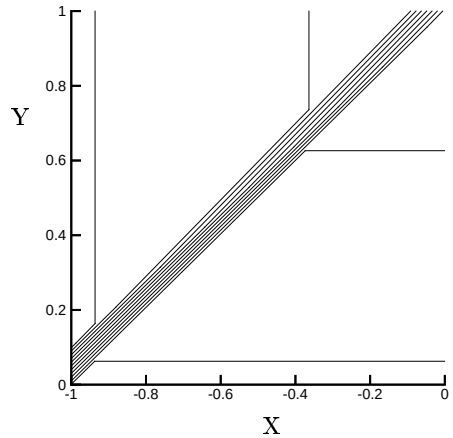

Fig. 5 Finite volume solution on the optimal fluctuation splitting mesh.

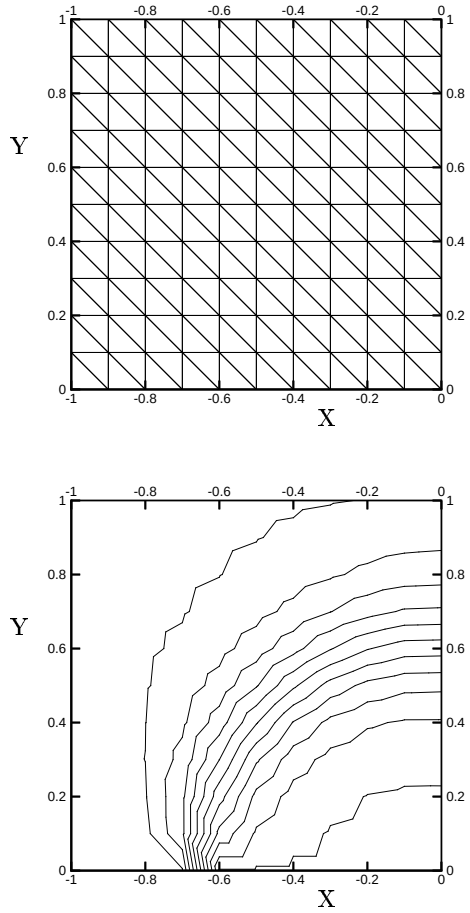

Fig. 6 Starting mesh and converged finite volume solution, $\vec{\lambda} = (y, -x)$. Solution contours vary on (0,1) with 0.1 increments.

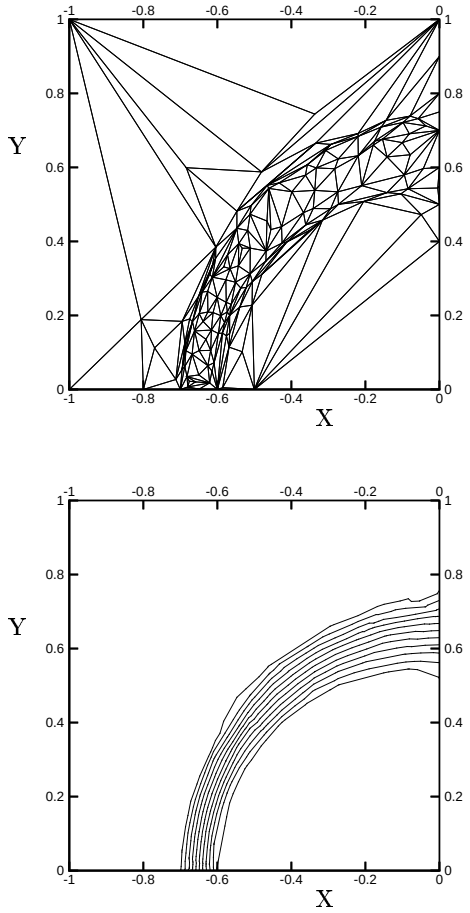

Fig. 7 Converged finite volume solution and curvature-clustered mesh after three grid-adaption cycles, $\vec{\lambda} = (y, -x)$. Solution contours vary on (0,1) with 0.1 increments.

very poor containment of the leading and trailing contour levels.

Circular Advection

The second case considered is for circular advection, with a variable advection velocity of $\vec{\lambda} = (y, -x)$. The inflow profile is $U(x, 0) = 0$ on $x = [-1, 0.7]$ and $U(x, 0) = 1$ on $x = [-0.6, 0]$. The initial mesh and highly diffused finite volume solution on this mesh are shown in Fig. 6. As before, the fluctuation splitting solution on this mesh is similar in character, though less diffusive than the finite volume result. Three adaption cycles of the curvature clustering with the finite volume solver are applied, leading to the mesh and solution of Fig. 7. The number of nodes has increased from 121 to 146, but the solution has been dramatically improved.

For this problem, an optimal mesh can be constructed following the characteristic-alignment guidelines. Such a mesh is shown in Fig. 8, along with the exact solution as computed by the fluctuation splitting solver. This mesh contains only 10 nodes. The finite volume solution on this mesh, Fig. 9, is clearly far inferior to the exact fluctuation splitting solution.

In practice, though, the local adaption algorithm for fluctuation splitting presented here is not able to reduce the mesh to the 'optimal' grid for this case. This is because each local operation is constrained to be in the direction of a local improvement only. In order to reduce the starting grid to the 'optimal' mesh, a global communication is required between nodes to know that a local move in the non-optimal direction will be counter-acted by changes occurring at another node. The present method is applied to the circular advection problem for one cycle, using four sub-iterates of the diagonalized Newton scheme during the nodal displacement step. The resulting mesh, containing 70 nodes, and fluctuation splitting solution are shown in Fig. 10. The fluctuation splitting result is of comparable accuracy, but rougher at the edges of the shear, to the adapted finite volume solution obtained on a grid containing twice as many points.

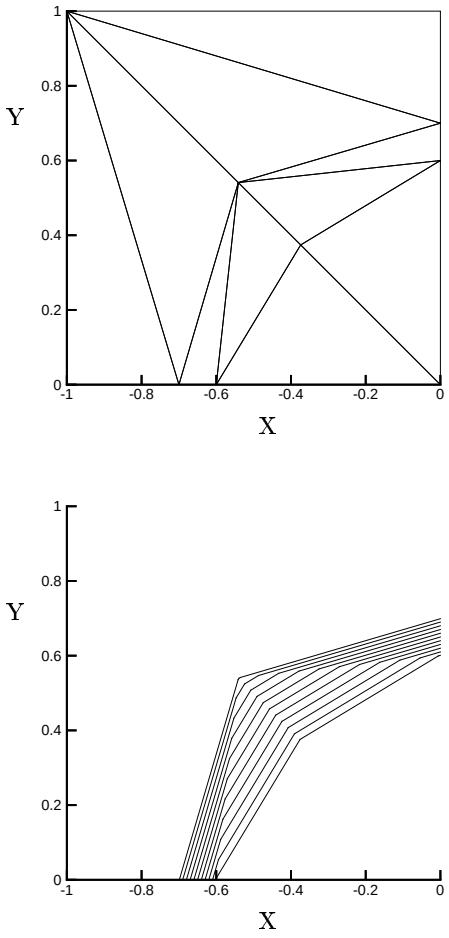

Fig. 8 Optimized mesh, created by hand, and exact solution to circular advection problem, using fluctuation splitting.

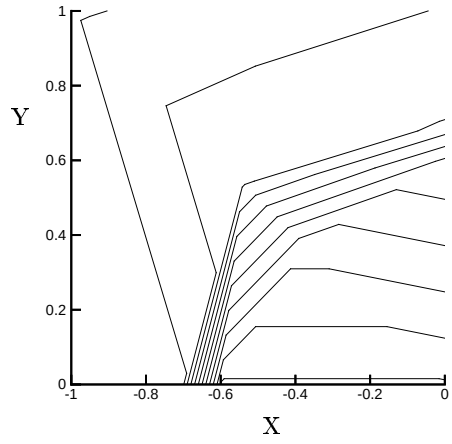

Fig. 9 Finite volume solution on the optimal fluctuation splitting mesh for circular advection.

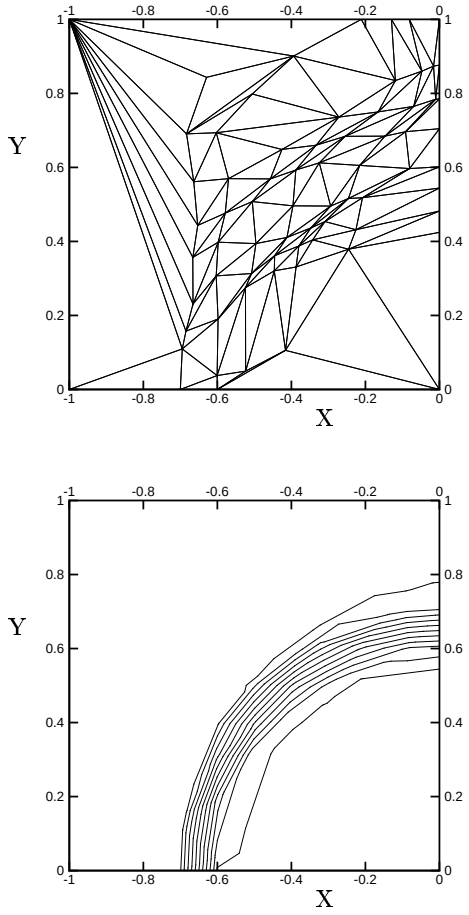

Fig. 10 Mesh and fluctuation splitting solution after one adaption cycle for circular advection. Contours vary on (0,1), with 0.1 increment.

Non-linear Advection

A non-linear advection case is constructed containing a symmetric compression fan that coalesces into a vertical shock at $(-\frac{1}{2}, \frac{1}{2})$. Centered expansion fans sit at (-1,0) and (0,0). The inflow profile is,

$$\begin{aligned} U(x,0) &= -2x - 1 \qquad \text{on } x = (-1,0) \\ U(-1,0) &= U(0,0) = 0 \end{aligned} \tag{43}$$

The unadapted mesh and extremely diffused finite volume solution are shown in Fig. 11. Three full cycles of the curvature-clustering adaption nearly double the number of nodes to 237, yielding the mesh and solution in Fig. 12. The solution on this mesh shows a dramatic improvement for shock thickness, shock speed, point of coalescence, and preservation of extremum in smooth regions. Note, however, that there is some asymmetry between the expansion fans toward the top of the domain, that the shock is not entirely straight, and that the compression fan begins to coalesce into a shock at $y = 0.4$, instead of at $y = 0.5$, the correct location.

The fluctuation splitting adaption scheme is also applied for three cycles to the same problem and ini-

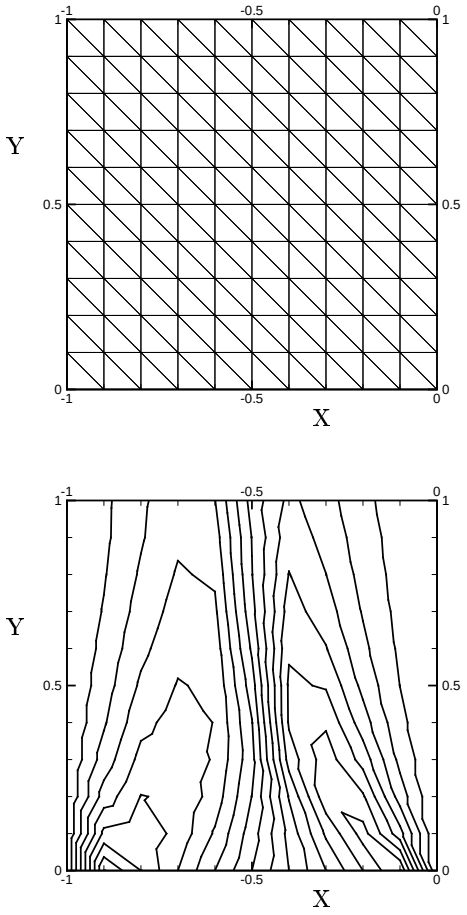

Fig. 11 Initial mesh and finite volume solution for non-linear advection case. Contours vary on (-1,1), with 0.1 increment.

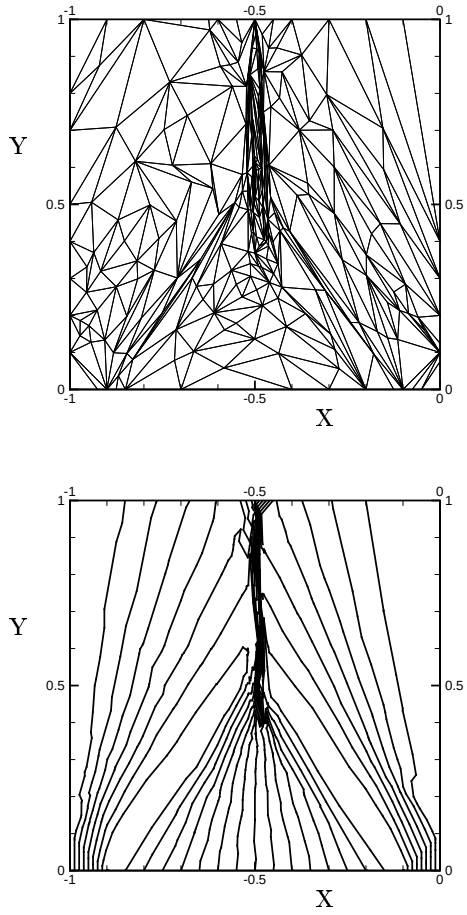

Fig. 12 Curvature-clustered mesh and finite volume solution after three adaption cycles, non-linear advection case. Contours vary on (-1,1), with 0.1 increment.

tial grid. The adapted mesh, containing 206 nodes, and corresponding solution are shown in Fig. 13. For this test case, there are pros and cons for both sets of results. The adapted fluctuation splitting solution, using 14 percent fewer nodes, exhibits slightly greater accuracy than the adapted finite volume solution, particularly in the expansion fan symmetry and shock coalescence point. One feature that is better resolved in the finite volume solution is the extremum between the compression and expansion fans on the lower right-hand side. The fluctuation splitting shock is broader near the coalescence point but tapers to a comparable crispness with the finite volume result, and is a little straighter. The fluctuation splitting shock at the outflow is ever so slightly offset to the right from $x = -0.5$, the correct location.

The finite volume and fluctuation splitting meshes, Figs. 12 and 13, have similar character in the expansion and compression fans. The fluctuation splitting adaption does not cluster as many points to the shock, resulting in overall 14 percent fewer nodes. This fact that the fluctuation splitting adaption scheme can resolve crisp shocks without excessive clustering normal to the shock may have favorable implications when considering fluid dynamic problems with extremely strong shocks in the vicinity of more subtle, though still important, features, such as an entropy layer.

Advection-Diffusion

The final case is for an advection-diffusion problem due to Smith and Hutton.[32] The advection velocity is,

$$\vec{\lambda} = \left(2y(1-x^2),\ -2x(1-y^2)\right) \tag{44}$$

The inflow profile is,

$$U(x,0) = 1 + \tanh(20x + 10) \tag{45}$$

The diffusion coefficient is chosen to be a small constant, $\mu = 10^{-3}$, to be representative of a high-Reynolds-number shear. The starting mesh for this case is an unstructured isotropic mesh containing 1928 nodes. The reference solution for this case is taken from a fully grid-converged solution on an isotropic mesh (20,000 nodes).[24] Both the finite volume and

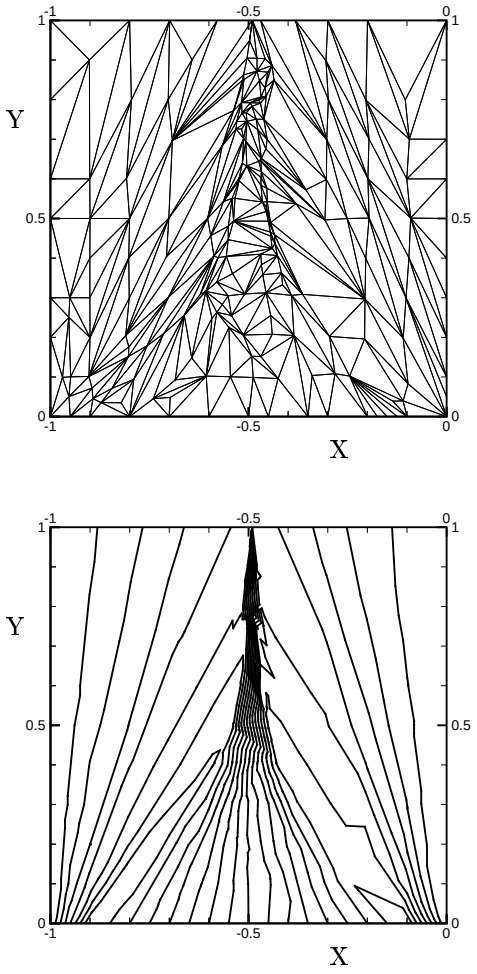

Fig. 13 Mesh and fluctuation splitting solution after three adaption cycles, non-linear advection case. Contours vary on (-1,1), with 0.1 increment.

fluctuation splitting solvers are run on the unadapted mesh, and the RMS difference in the outflow profiles between these solutions on the starting mesh and the fully-resolved solution are compared in table 1. As usual, the fluctuation splitting solution is seen to be more accurate than the finite volume solver on the unadapted mesh.

Two cycles of curvature-clustering adaption are applied, reducing the number of nodes by two-thirds to 619, while improving the RMS outflow resolution by 28 percent, also listed in table 1. One cycle of the fluctuation splitting adaption reduces the number of nodes to 695, while still producing some (7 percent) improvement in accuracy.

Concluding Remarks

Current state of the art for local anisotropic unstructured mesh adaption based on *a posteriori* error estimates has been implemented in an edge-based structure in conjunction with a finite volume solver. This type of adaption results in meshes where the node densities are clustered to regions of high curvature in the solution. Significant improvement in solution accuracy is verified using this technique on scalar model problems.

Table 1 RMS difference of solution outflow profile relative to reference solution.

	Finite volume	Fluctuation splitting
unadapted	0.0288	0.0068
adapted	0.0208	0.0063

Recognizing the remarkable property of the discretized fluctuation splitting scheme that multi-dimensional advection can be solved exactly when one edge of each cell is aligned with the characteristic direction, a different mesh adaption scheme is proposed. While retaining the mechanics of performing only local operations, *i.e.* point insertion/deletion, edge swapping, and nodal displacement, a solution-predictive approach is chosen in favor of *a posteriori* curvature clustering. The concept of aligning cell edges with characteristic directions is generalized as a minimization procedure to allow extension to diffusion problems and systems. Extending this process to non-linear problems led to an implementation of eigenvalue limiting for multi-dimensional upwind distribution schemes.

It is seen that, while performing a series of local optimizations does lead to globally improved solution accuracy and reduced grid sizes, in general a truly globally 'optimal' mesh is not achieved in a small number of adaption cycles. However, the solution-predictive adaption in conjunction with the fluctuation splitting scheme does provide moderately more accurate solutions on smaller meshes for comparable number of adaption cycles versus the finite volume solver with adaption driven by error estimates.

Considering extensions to three-dimensional hypersonic flow applications, perhaps the most promising difference between the two adaption strategies lies in their treatment of shocks. For the *a posteriori* adaption, the number of nodes clustered to the shock grows as the shock strength grows, which can lead to a bow shock dominating the adaption for hypersonic problems. In contrast, the minimization of fluctuations tends to merely align the grid with the shock, leaving the points outside the shock largely unaffected.

Appendix

The variations of the cell fluctuations and the dependent variable nodal values with respect to changes in the nodal location are developed for the advective distribution scheme of Sidilkover and the diffusive Galerkin distribution.

Advective Fluctuations

The advective fluctuation can be manipulated from Eqn. 17 as,

$$\phi = \frac{1}{2}\left[(U_2 - U_3)(y_1,\, -x_1) + (U_3 - U_1)(y_2,\, -x_2) + (U_1 - U_2)(y_3,\, -x_3)\right]\cdot\tilde{\vec{A}} \quad (46)$$

The spatial derivatives take the form,

$$\frac{\partial\phi}{\partial x_2} = \frac{1}{2}\left[(U_1 - U_3)\tilde{A}^{\mathsf{y}} + \sum_{j=1}^{3} U_j \ell_j \hat{n}_j \cdot \frac{\partial\tilde{\vec{A}}}{\partial x_2} + \sum_{j=1}^{3} \ell_j \hat{n}_j \cdot \tilde{\vec{A}} \frac{\partial U_j}{\partial x_2}\right] \quad (47)$$

$$\frac{\partial\phi}{\partial y_2} = \frac{1}{2}\left[(U_3 - U_1)\tilde{A}^{\mathsf{x}} + \sum_{j=1}^{3} U_j \ell_j \hat{n}_j \cdot \frac{\partial\tilde{\vec{A}}}{\partial y_2} + \sum_{j=1}^{3} \ell_j \hat{n}_j \cdot \tilde{\vec{A}} \frac{\partial U_j}{\partial y_2}\right] \quad (48)$$

The derivatives of the cell-averaged flux Jacobian will depend upon the particular flux function. However, since $\tilde{\vec{A}}$ is a weighted average of three nodal values,

$$\frac{\partial\tilde{\vec{A}}}{\partial x_2} \sim \frac{1}{3}\frac{\partial\vec{A}_2}{\partial x_2} \quad (49)$$

For uniform advection, $\frac{\partial\tilde{\vec{A}}}{\partial x_2} = 0$. For circular advection, $\frac{\partial\tilde{\vec{A}}}{\partial x_2} = (0, -\frac{1}{3})$ and $\frac{\partial\tilde{\vec{A}}}{\partial y_2} = (\frac{1}{3}, 0)$. For non-linear problems, in general,

$$\frac{\partial\tilde{\vec{A}}}{\partial x_2} \sim \frac{1}{3}\frac{\partial U_2}{\partial x_2} \quad (50)$$

In keeping with the Gauß-Seidel update philosophy, only the derivative of the solution value at the current node is retained in the last term of Eqns. 47 and 48. That is, if the current node is designated node 2 of the triangle under consideration, then $\frac{\partial U_2}{\partial x_2} = \frac{\partial U_i}{\partial x_i}$ is retained while $\frac{\partial U_1}{\partial x_2} \simeq \frac{\partial U_3}{\partial x_2} \simeq 0$ is assumed.

Second derivatives of the advective fluctuation with respect to variation of a nodal location follow from Eqns. 47 and 48, incorporating the approximation $\frac{\partial U_1}{\partial x_2} \simeq \frac{\partial U_3}{\partial x_2} \simeq 0$,

$$\frac{\partial^2\phi}{\partial x_2^2} = (U_1 - U_3)\frac{\partial\tilde{A}^{\mathsf{y}}}{\partial x_2} + \ell_2\hat{n}_2\cdot\frac{\partial\tilde{\vec{A}}}{\partial x_2}\frac{\partial U_2}{\partial x_2} + \frac{\ell_2}{2}\hat{n}_2\cdot\tilde{\vec{A}}\frac{\partial^2 U_2}{\partial x_2^2} + \sum_{j=1}^{3} U_j\frac{\ell_j}{2}\hat{n}_j\cdot\frac{\partial^2\tilde{\vec{A}}}{\partial x_2^2} \quad (51)$$

$$\frac{\partial^2\phi}{\partial y_2^2} = (U_3 - U_1)\frac{\partial\tilde{A}^{\mathsf{x}}}{\partial y_2} + \ell_2\hat{n}_2\cdot\frac{\partial\tilde{\vec{A}}}{\partial y_2}\frac{\partial U_2}{\partial y_2} + \frac{\ell_2}{2}\hat{n}_2\cdot\tilde{\vec{A}}\frac{\partial^2 U_2}{\partial y_2^2} + \sum_{j=1}^{3} U_j\frac{\ell_j}{2}\hat{n}_j\cdot\frac{\partial^2\tilde{\vec{A}}}{\partial y_2^2} \quad (52)$$

$$\frac{\partial^2\phi}{\partial x_2\partial y_2} = \frac{1}{2}\left[(U_3 - U_1)\left(\frac{\partial\tilde{A}^{\mathsf{x}}}{\partial x_2} - \frac{\partial\tilde{A}^{\mathsf{y}}}{\partial y_2}\right) + \ell_2\hat{n}_2\cdot\left(\frac{\partial\tilde{\vec{A}}}{\partial y_2}\frac{\partial U_2}{\partial x_2} + \frac{\partial\tilde{\vec{A}}}{\partial x_2}\frac{\partial U_2}{\partial y_2}\right) + \ell_2\hat{n}_2\cdot\tilde{\vec{A}}\frac{\partial^2 U_2}{\partial x_2\partial y_2} + \sum_{j=1}^{3} U_j\ell_j\hat{n}_j\cdot\frac{\partial^2\tilde{\vec{A}}}{\partial x_2\partial y_2}\right] \quad (53)$$

Second derivatives of $\tilde{\vec{A}}$ are developed in an analogous manner to its first derivatives.

Diffusive Fluctuations

Derivatives of the diffusive fluctuations take the form,

$$\frac{\partial\phi_2^v}{\partial x_2} = -\frac{\bar{\mu}}{4S_{\mathsf{T}}}\left[\left(\frac{1}{\bar{\mu}}\frac{\partial\bar{\mu}}{\partial x_2} - \frac{1}{S_{\mathsf{T}}}\frac{\partial S_{\mathsf{T}}}{\partial x_2}\right)\sum_{j=1}^{3} U_j\ell_j\ell_2\hat{n}_j\cdot\hat{n}_2 + \ell_2^2\frac{\partial U_2}{\partial x_2} + (x_3 - x_1)(U_1 - U_3)\right] \quad (54)$$

$$\frac{\partial\phi_2^v}{\partial y_2} = -\frac{\bar{\mu}}{4S_{\mathsf{T}}}\left[\left(\frac{1}{\bar{\mu}}\frac{\partial\bar{\mu}}{\partial y_2} - \frac{1}{S_{\mathsf{T}}}\frac{\partial S_{\mathsf{T}}}{\partial y_2}\right)\sum_{j=1}^{3} U_j\ell_j\ell_2\hat{n}_j\cdot\hat{n}_2 + \ell_2^2\frac{\partial U_2}{\partial y_2} + (y_3 - y_1)(U_1 - U_3)\right] \quad (55)$$

where the assumption $\frac{\partial U_1}{\partial x_2} \simeq \frac{\partial U_3}{\partial x_2} \simeq 0$ has already been applied. The second derivatives of the diffusive distribution follow as,

$$\frac{\partial^2\phi_2^v}{\partial x_2^2} = -\frac{\bar{\mu}\ell_2^2}{4S_{\mathsf{T}}}\frac{\partial^2 U_2}{\partial x_2^2} + \left(\frac{\bar{\mu}}{4S_{\mathsf{T}}^2}\frac{\partial S_{\mathsf{T}}}{\partial x_2} - \frac{1}{4S_{\mathsf{T}}}\frac{\partial\bar{\mu}}{\partial x_2}\right)\cdot\left[\ell_2^2\frac{\partial U_2}{\partial x_2} + (x_3 - x_1)(U_1 - U_3)\right] + \left[\frac{1}{4\bar{\mu}S_{\mathsf{T}}}\left(\frac{\partial\bar{\mu}}{\partial x_2}\right)^2 - \frac{1}{4S_{\mathsf{T}}}\frac{\partial^2\bar{\mu}}{\partial x_2^2} + \frac{\bar{\mu}}{4S_{\mathsf{T}}^2}\frac{\partial^2 S_{\mathsf{T}}}{\partial x_2^2} - \frac{\bar{\mu}}{4S_{\mathsf{T}}^3}\left(\frac{\partial S_{\mathsf{T}}}{\partial x_2}\right)^2\right]\cdot\sum_{j=1}^{3} U_j\ell_j\ell_2\hat{n}_j\cdot\hat{n}_2 + \left(\frac{1}{\bar{\mu}}\frac{\partial\bar{\mu}}{\partial x_2} - \frac{1}{S_{\mathsf{T}}}\frac{\partial S_{\mathsf{T}}}{\partial x_2}\right)\frac{\partial\phi_2^v}{\partial x_2} \quad (56)$$

$$\frac{\partial^2\phi_2^v}{\partial y_2^2} = -\frac{\bar{\mu}\ell_2^2}{4S_\mathsf{T}}\frac{\partial^2 U_2}{\partial y_2^2} + \left(\frac{\bar{\mu}}{4S_\mathsf{T}^2}\frac{\partial S_\mathsf{T}}{\partial y_2} - \frac{1}{4S_\mathsf{T}}\frac{\partial \bar{\mu}}{\partial y_2}\right)\cdot \left[\ell_2^2\frac{\partial U_2}{\partial y_2} + (y_3 - y_1)(U_1 - U_3)\right] + \left[\frac{1}{4\bar{\mu}S_\mathsf{T}}\left(\frac{\partial \bar{\mu}}{\partial y_2}\right)^2 - \frac{1}{4S_\mathsf{T}}\frac{\partial^2\bar{\mu}}{\partial y_2^2} + \frac{\bar{\mu}}{4S_\mathsf{T}^2}\frac{\partial^2 S_\mathsf{T}}{\partial y_2^2} - \frac{\bar{\mu}}{4S_\mathsf{T}^3}\left(\frac{\partial S_\mathsf{T}}{\partial y_2}\right)^2\right]\cdot \sum_{j=1}^{3} U_j\ell_j\ell_2\hat{n}_j\cdot\hat{n}_2 + \left(\frac{1}{\bar{\mu}}\frac{\partial\bar{\mu}}{\partial y_2} - \frac{1}{S_\mathsf{T}}\frac{\partial S_\mathsf{T}}{\partial y_2}\right)\frac{\partial\phi_2^v}{\partial y_2} \quad (57)$$

$$\frac{\partial^2\phi_2^v}{\partial x_2\partial y_2} = -\frac{\bar{\mu}\ell_2^2}{4S_\mathsf{T}}\frac{\partial^2 U_2}{\partial x_2\partial y_2} + \left(\frac{\bar{\mu}}{4S_\mathsf{T}^2}\frac{\partial S_\mathsf{T}}{\partial x_2} - \frac{1}{4S_\mathsf{T}}\frac{\partial \bar{\mu}}{\partial x_2}\right)\cdot \left[\ell_2^2\frac{\partial U_2}{\partial y_2} + (y_3 - y_1)(U_1 - U_3)\right] + \left(\frac{1}{4\bar{\mu}S_\mathsf{T}}\frac{\partial\bar{\mu}}{\partial x_2}\frac{\partial\bar{\mu}}{\partial y_2} - \frac{1}{4S_\mathsf{T}}\frac{\partial^2\bar{\mu}}{\partial x_2\partial y_2} + \frac{\bar{\mu}}{4S_\mathsf{T}^2}\frac{\partial^2 S_\mathsf{T}}{\partial x_2\partial y_2} - \frac{\bar{\mu}}{4S_\mathsf{T}^3}\frac{\partial S_\mathsf{T}}{\partial x_2}\frac{\partial S_\mathsf{T}}{\partial y_2}\right)\cdot \sum_{j=1}^{3} U_j\ell_j\ell_2\hat{n}_j\cdot\hat{n}_2 + \left(\frac{1}{\bar{\mu}}\frac{\partial\bar{\mu}}{\partial y_2} - \frac{1}{S_\mathsf{T}}\frac{\partial S_\mathsf{T}}{\partial y_2}\right)\frac{\partial\phi_2^v}{\partial x_2} \quad (58)$$

The derivatives of the cell-averaged diffusion coefficient scale like,

$$\frac{\partial\bar{\mu}}{\partial x_2} \sim \frac{1}{3}\frac{\partial\mu_2}{\partial x_2} \qquad \frac{\partial^2\bar{\mu}}{\partial x_2^2} \sim \frac{1}{3}\frac{\partial^2\mu_2}{\partial x_2^2} \quad (59)$$

Dependent Variable

Evaluating $\frac{\partial U_i}{\partial x_i}$ directly from the high-resolution non-linear fluctuation splitting scheme is impractical. Limiters such as Minmod are not continuously differentiable, and while the van Albada limiter is differentiable its use does not lead to a convenient explicit form from which to evaluate $\frac{\partial U_i}{\partial x_i}$. As an approximation to $\frac{\partial U_i}{\partial x_i}$ for the non-linear scheme, derivatives are sought using linear distribution schemes. Two linear choices for fluctuation splitting are to use a linearity preserving (second-order spatial accuracy), non-monotonic distribution or an upwind, monotonic first-order distribution. The linearity-preserving, non-monotonic scheme is of the Lax-Wendroff type,[33] and tends to produce dispersion waves in response to nodal displacements. This behavior tends to under-predict the change in solution value at the perturbed node relative to the fluctuation splitting scheme employed herein.

The linear upwind scheme is obtained from the present fluctuation splitting scheme by discarding the limiter. This scheme exhibits a dependency on the numbering of nodes within a triangle. To alleviate this dependency, the approximation to $\frac{\partial U_i}{\partial x_i}$ is built by looping over all cells connected to node i and locally renumbering the nodes within each triangle so that the current node is designated as node 2 of the triangle. It is emphasized that the linear upwind scheme is not used in the calculation of the solution, but only employed to provide an estimate of the solution variation with respect to nodal displacements, providing the forcing functions for the mesh adaption.

Assembling the linear upwind advective distributions with the diffusive contributions from the surrounding cells and solving for the steady state value of the current node yields, with $U_2 = U_i$,

$$U_i\sum_{\mathsf{T}}\left(\alpha^+ - \beta^- + \frac{\bar{\mu}\ell_i^2}{4S_\mathsf{T}}\right) = \sum_{\mathsf{T}}\left[\alpha^+U_1 - \beta^-U_3 - \frac{\bar{\mu}\ell_i}{4S_\mathsf{T}}\left(U_1\ell_1\hat{n}_1 + U_3\ell_3\hat{n}_3\right)\cdot\hat{n}_i\right] \quad (60)$$

where,

$$\alpha^\pm = \frac{\alpha \pm |\alpha|}{2} = \alpha\frac{1 \pm \mathrm{sign}(\alpha)}{2}$$
$$\beta^\pm = \frac{\beta \pm |\beta|}{2} = \beta\frac{1 \pm \mathrm{sign}(\beta)}{2} \quad (61)$$

The variation of the nodal solution with respect to nodal displacement can now be evaluated as,

$$\frac{\partial U_i}{\partial x_i}\sum_{\mathsf{T}}\left(\alpha^+ - \beta^- + \frac{\bar{\mu}\ell_2^2}{4S_\mathsf{T}}\right) = \sum_{\mathsf{T}}\left\{U_1\frac{\partial\alpha^+}{\partial x_i} - U_3\frac{\partial\beta^-}{\partial x_i} - \frac{\bar{\mu}}{4S_\mathsf{T}}\left[\ell_i\left(\frac{1}{\bar{\mu}}\frac{\partial\bar{\mu}}{\partial x_i} - \frac{1}{S_\mathsf{T}}\frac{\partial S_\mathsf{T}}{\partial x_i}\right)\left(U_1\ell_1\hat{n}_1\cdot\hat{n}_i + U_3\ell_3\hat{n}_3\cdot\hat{n}_i\right) + (x_3 - x_1)(U_1 - U_3)\right]\right\} - U_i\sum_{\mathsf{T}}\left(\frac{\partial\alpha^+}{\partial x_i} - \frac{\partial\beta^-}{\partial x_i} + \frac{\ell_i^2}{4S_\mathsf{T}}\frac{\partial\bar{\mu}}{\partial x_i} - \frac{\ell_i^2\bar{\mu}}{4S_\mathsf{T}^2}\frac{\partial S_\mathsf{T}}{\partial x_i}\right) \quad (62)$$

Recall that the solution at surrounding nodes is held fixed during displacements of the current node.

The derivatives of the functions in Eqn. 61 are defined,

$$\frac{\partial\alpha^+}{\partial x} = \begin{cases} 0, & \alpha < 0 \\ \frac{\partial\alpha}{\partial x}, & \alpha \geq 0 \end{cases}, \quad \frac{\partial\beta^-}{\partial x} = \begin{cases} \frac{\partial\beta}{\partial x}, & \beta \leq 0 \\ 0, & \beta > 0 \end{cases} \quad (63)$$

Further, Eqn. 10 leads to,

$$\frac{\partial\alpha}{\partial x_2} = \frac{\tilde{A}^\mathsf{y}}{2} + \frac{1}{2}\ell_1\hat{n}_1\cdot\frac{\partial\tilde{\vec{A}}}{\partial x_2}, \quad \frac{\partial\alpha}{\partial y_2} = -\frac{\tilde{A}^\mathsf{x}}{2} + \frac{1}{2}\ell_1\hat{n}_1\cdot\frac{\partial\tilde{\vec{A}}}{\partial y_2} \quad (64)$$

$$\frac{\partial\beta}{\partial x_2} = \frac{\tilde{A}^\mathsf{y}}{2} - \frac{1}{2}\ell_3\hat{n}_3\cdot\frac{\partial\tilde{\vec{A}}}{\partial x_2}, \quad \frac{\partial\beta}{\partial y_2} = -\frac{\tilde{A}^\mathsf{x}}{2} - \frac{1}{2}\ell_3\hat{n}_3\cdot\frac{\partial\tilde{\vec{A}}}{\partial y_2} \quad (65)$$

For non-linear problems a circular definition arises for $\frac{\partial U_i}{\partial x_i}$ and $\frac{\partial\tilde{\vec{A}}}{\partial x_i}$. One option is to neglect the derivatives of $\tilde{\vec{A}}$ in Eqns. 64 and 65. Another option would be to lag these same terms from the previous iteration level.

The second derivatives of the solution at the current node with respect to variations in the position of the

current node can be developed from the first derivative expression in Eqn. 62, again with the approximation $\frac{\partial U_1}{\partial x_2} \simeq \frac{\partial U_3}{\partial x_2} \simeq 0$,

$$\frac{\partial^2 U_i}{\partial x_i^2} \sum_{\mathsf{T}} \left(\alpha^+ - \beta^- + \frac{\bar{\mu}\ell_i^2}{4S_{\mathsf{T}}} \right) = - U_i \sum_{\mathsf{T}} \frac{\partial^2}{\partial x_i^2} \left(\alpha^+ \beta^- + \frac{\bar{\mu}\ell_i^2}{4S_{\mathsf{T}}} \right) + \sum_{\mathsf{T}} \left[U_1 \frac{\partial^2 \alpha^+}{\partial x_i^2} - U_3 \frac{\partial^2 \beta^-}{\partial x_i^2} - 2\ell_i (U_1 - U_3)(x_3 - x_1) \frac{\partial}{\partial x_i} \left(\frac{\bar{\mu}}{4S_{\mathsf{T}}} \right) \right] - 2\frac{\partial U_i}{\partial x_i} \sum_{\mathsf{T}} \frac{\partial}{\partial x_i} \left(\alpha^+ - \beta^- + \frac{\bar{\mu}\ell_i^2}{4S_{\mathsf{T}}} \right) \quad (66)$$

$$\frac{\partial^2 U_i}{\partial x_i \partial y_i} \sum_{\mathsf{T}} \left(\alpha^+ - \beta^- + \frac{\bar{\mu}\ell_i^2}{4S_{\mathsf{T}}} \right) = - U_i \sum_{\mathsf{T}} \frac{\partial^2}{\partial x_i \partial y_i} \left(\alpha^+ - \beta^- + \frac{\bar{\mu}\ell_i^2}{4S_{\mathsf{T}}} \right) - \frac{\partial U_i}{\partial x_i} \sum_{\mathsf{T}} \frac{\partial}{\partial y_i} \left(\alpha^+ - \beta^- + \frac{\bar{\mu}\ell_i^2}{4S_{\mathsf{T}}} \right) + \sum_{\mathsf{T}} \left(U_1 \frac{\partial^2 \alpha^+}{\partial x_i \partial y_i} - U_3 \frac{\partial^2 \beta^-}{\partial x_i \partial y_i} \right) - \sum_{\mathsf{T}} \left\{ \ell_i (U_1 - U_3) \cdot \left[(x_3 - x_1) \frac{\partial}{\partial y_i} \left(\frac{\bar{\mu}}{4S_{\mathsf{T}}} \right) + (y_3 - y_1) \frac{\partial}{\partial x_i} \left(\frac{\bar{\mu}}{4S_{\mathsf{T}}} \right) \right] \right\} - \frac{\partial U_i}{\partial y_i} \sum_{\mathsf{T}} \frac{\partial}{\partial x_i} \left(\alpha^+ - \beta^- + \frac{\bar{\mu}\ell_i^2}{4S_{\mathsf{T}}} \right) \quad (67)$$

The remaining derivatives to be specified follow from Eqns. 64 and 65,

$$\frac{\partial^2 \alpha}{\partial x_2^2} = \frac{\partial \tilde{A}^{\mathsf{y}}}{\partial x_2} + \frac{1}{2}\ell_1 \hat{n}_1 \cdot \frac{\partial^2 \tilde{\vec{A}}}{\partial x_2^2} \quad (68)$$

$$\frac{\partial^2 \alpha}{\partial y_2^2} = -\frac{\partial \tilde{A}^{\mathsf{x}}}{\partial y_2} + \frac{1}{2}\ell_1 \hat{n}_1 \cdot \frac{\partial^2 \tilde{\vec{A}}}{\partial y_2^2} \quad (69)$$

$$\frac{\partial^2 \alpha}{\partial x_2 \partial y_2} = \frac{1}{2}\frac{\partial \tilde{A}^{\mathsf{y}}}{\partial y_2} - \frac{1}{2}\frac{\partial \tilde{A}^{\mathsf{x}}}{\partial x_2} + \frac{1}{2}\ell_1 \hat{n}_1 \cdot \frac{\partial^2 \tilde{\vec{A}}}{\partial x_2 \partial y_2} \quad (70)$$

$$\frac{\partial^2 \beta}{\partial x_2^2} = \frac{\partial \tilde{A}^{\mathsf{y}}}{\partial x_2} - \frac{1}{2}\ell_3 \hat{n}_3 \cdot \frac{\partial^2 \tilde{\vec{A}}}{\partial x_2^2} \quad (71)$$

$$\frac{\partial^2 \beta}{\partial y_2^2} = -\frac{\partial \tilde{A}^{\mathsf{x}}}{\partial y_2} - \frac{1}{2}\ell_3 \hat{n}_3 \cdot \frac{\partial^2 \tilde{\vec{A}}}{\partial y_2^2} \quad (72)$$

$$\frac{\partial^2 \beta}{\partial x_2 \partial y_2} = \frac{1}{2}\frac{\partial \tilde{A}^{\mathsf{y}}}{\partial y_2} - \frac{1}{2}\frac{\partial \tilde{A}^{\mathsf{x}}}{\partial x_2} - \frac{1}{2}\ell_3 \hat{n}_3 \cdot \frac{\partial^2 \tilde{\vec{A}}}{\partial x_2 \partial y_2} \quad (73)$$

References

[1]Kleb, W. L., Wood, W. A., Gnoffo, P. A., and Alter, S. J., "Computational Aeroheating Predictions for X-34," *Journal of Spacecraft and Rockets*, Vol. 36, No. 2, March 1999, pp. 179–188.

[2]Gnoffo, P. A., "A Finite-Volume, Adaptive Grid Algorithm Applied to Planetary Entry Flowfields," *AIAA Journal*, Vol. 21, No. 9, Sept. 1983, pp. 1249–1254.

[3]Harvey, A. D., Acharya, S., Lawrence, S. L., and Cheung, S., "A Solution Adaptive Grid Procedure for an Upwind Parabolized Flow Solver," AIAA Paper 90–1567, June 1990.

[4]Harvey, A. D., Acharya, S., and Lawrence, S. L., "A Solution-Adaptive Grid Procedure for the Three-Dimensional Parabolized Navier-Stokes Equations," AIAA Paper 91–0104, January 1991.

[5]Harvey, A. D., Acharya, S., and Lawrence, S. L., "Prediction of Complex Three-Dimensional Flowfields Using a Solution-Adaptive Mesh Algorithm," AIAA Paper 91-3237, September 1991.

[6]Hétu, J.-F. and Pelletier, D. H., "Adaptive Remeshing for Viscous Incompressible Flows," *AIAA Journal*, Vol. 30, No. 8, Aug. 1992, pp. 1986–1992.

[7]Hétu, J.-F. and Pelletier, D. H., "Fast, Adaptive Finite Element Scheme for Viscous Incompressible Flows," *AIAA Journal*, Vol. 30, No. 11, Nov. 1992, pp. 2677–2682.

[8]Parthasarathy, V. and Kallinderis, Y., "Adaptive Prismatic-Tetrahedral Grid Refinement and Redistribution for Viscous Flows," *AIAA Journal*, Vol. 34, No. 4, April 1996, pp. 707–716.

[9]Marcum, D. L., "Adaptive Unstructured Grid Generation for Viscous Flow Applications," *AIAA Journal*, Vol. 34, No. 11, Nov. 1996, pp. 2440–2443.

[10]Ilinca, F., Pelletier, D., and Ignat, L., "Adaptive Finite Element Solution of Compressible Turbulent Flows," AIAA Paper 98–0229, Jan. 1998.

[11]Turgeon, E., Pelletier, D., and Ignat, L., "Effects of Adaptivity on Various Finite Element Schemes for Turbulent Heat Transfer and Flow Predictions," AIAA Paper 98–0853, Jan. 1998.

[12]Dompierre, J., Vallet, M.-G., Fortin, M., Bourgault, Y., and Habashi, W. G., "Anisotropic Mesh Adaption: Towards a Solver and User Independent CFD," AIAA Paper 97–0861, Jan. 1997.

[13]Taghaddosi, F., Habashi, W. G., Guèvremont, G., and Ait-Ali-Yahia, D., "An Adaptive Least-Squares Method for the Compressible Euler Equations," AIAA Paper 97–2097, June 1997.

[14]Ait-Ali-Yahia, D. and Habashi, W. G., "Finite Element Adaptive Method for Hypersonic Thermochemical Nonequilibrium Flows," *AIAA Journal*, Vol. 35, No. 8, Aug. 1997, pp. 1294–1302.

[15]Habashi, W. G., Fortin, M., Dompierre, J., Vallet, M.-G., and Bourgault, Y., "Anisotropic Mesh Adaption: A Step Towards a Mesh-Independent and User-Independent CFD," *Barriers and Challenges in Computational Fluid Dynamics*, edited by V. Venkatakrishnan et al, Kluwer Academic Publisher, 1998, pp. 99–117.

[16]Tam, A., Robichaud, M. P., Tremblay, P., Habashi, W. G., Hohmeyer, M., Guèvremont, G., Peeters, M. G., and Germain, P., "A 3-D Adaptive Anisotropic Method for External and Internal Flows," AIAA Paper 98–0771, Jan. 1998.

[17]Habashi, W. G., Dompierre, J., Bourgault, Y., Fortin, M., and Vallet, M.-G., "Certifiable Computational Fluid Dynamics Through Mesh Optimization," *AIAA Journal*, Vol. 36, No. 5, May 1998, pp. 703–711.

[18]Zienkiewicz, O. C. and Zhu, J. Z., "The Superconvergent Patch Recovery and *A Posteriori* Error Estimates. Part 1: The Recovery Technique," *International Journal for Numerical Methods in Engineering*, Vol. 33, 1992, pp. 1331–1364.

[19]Zienkiewicz, O. C. and Zhu, J. Z., "The Superconvergent Patch Recovery and *A Posteriori* Error Estimates. Part 2: Error Estimates and Adaptivity," *International Journal for Numerical Methods in Engineering*, Vol. 33, 1992, pp. 1365–1382.

[20]Ait-Ali-Yahia, D., Habashi, W. G., and Tam, A., "A Directionally Adaptive Methodology using and Edge-Based Error Estimate on Quadrilateral Grids," *International Journal for Numerical Methods in Fluids*, Vol. 23, 1996, pp. 673–690.

[21]Roe, P. L., "Fluctuation Splitting Schemes on Optimal Grids," AIAA Paper 97–2034, June 1997.

[22]Roe, P., "Compounded of Many Simples," *Barriers and Challenges in Computational Fluid Dynamics*, edited by V. Venkatakrishnan et al, Kluwer Academic Publishers, 1998, pp. 241–258.

[23]Spekreijse, S., "Multigrid Solution of Monotone Second-Order Discretization of Hyperbolic Conservation Laws," *Mathematics of Computation*, Vol. 49, 1987, pp. 135–155.

[24]Wood, W. A. and Kleb, W. L., "Diffusion Characteristics of Finite Volume and Fluctuation Splitting Schemes," *Journal of Computational Physics*, (accepted for publication) 1999.

[25]Wood, W. A. and Kleb, W. L., "Diffusion Characteristics of Upwind Schemes on Unstructured Triangulations," AIAA Paper 98–2443, June 1998.

[26]Roe, P. L., "Characteristic-Based Schemes for the Euler Equations," *Annual Review of Fluid Mechanics*, Vol. 18, 1986, pp. 337–365.

[27]Barth, T. J., "Aspects of Unstructured Grids and Finite-Volume Solvers for the Euler and Navier-Stokes Equations," *Computational Fluid Dynamics*, No. 1994–04 in Lecture Series, von Karman Institute for Fluid Dynamics, 1994.

[28]Sidilkover, D., "A Genuinely Multidimensional Upwind Scheme and Efficient Multigrid Solver for the Compressible Euler Equations," Report 94–84, ICASE, USA, Nov. 1994.

[29]Harten, A. and Hyman, J. M., "Self Adjusting Grid Methods for One-Dimensional Hyperbolic Conservation Laws," *Journal of Computational Physics*, Vol. 50, 1983, pp. 235–269.

[30]Zhang, H., Trépanier, J. Y., Reggio, M., and Camarero, R., "A Navier-Stokes Solver for Stretched Triangular Grids," AIAA Paper 92–0183, Jan. 1992.

[31]Wood, W. A. and Kleb, W. L., "Comments on the Diffusive Behavior of Two Upwind Schemes," NASA/TM 1998–208738, Oct. 1998.

[32]Smith, R. M. and Hutton, A. G., "The Numerical Treatment of Advection: A Performance Comparison of Current Methods," *Numerical Heat Transfer*, Vol. 5, 1982, pp. 439–461.

[33]Paillère, H., Deconinck, H., and van der Weide, E., "Upwind Residual Distribution Methods for Compressible Flow: An Alternative to Finite Volume and Finite Element Methods. Part I: Scalar Schemes," *Computational Fluid Dynamics*, No. 1997–02 in Lecture Series, von Karman Institute, Belgium, March 1997.